Dynamical Systems, and Space Mission Design

Jerry Marsden

Martin Lo (JPL), Wang-Sang Koon and Shane Ross (Caltech)

Control and Dynamical Systems and JPL
California Institute of Technology

CDS 270-1, Lecture 3A, April 10, 2000

marsden@cds.caltech.edu
http://www.cds.caltech.edu/~marsden/

Outline for Lecture 3A

- Homoclinic points.
- Horseshoes and chaos (informal introduction).
- Transversal Homoclinic Orbits in the PCR3BP.
- Homoclinic-Heteroclinic Chain in the PCR3BP.

Pendulum and Forced Pendulum

- We will introduce some of the basic ideas using the forced pendulum.
- ***Reference***:
  P. Holmes [1990] Poincaré, Celestial Mechanics, Dynamical Systems Theory and Chaos, *Physics Reports* **193**, 137–163.
- Forcing, Poincaré maps and transversal homoclinic points
- Discussion of the equation

$$\ddot{x} + \sin x = \epsilon \cos \omega t$$

- Distinction between the forced pendulum and the pendulum coupled to an oscillator.
- horseshoe map

- Conley-Moser Conditions: horizontal and vertical rectangles and uniform contraction, will be explained in the next lecture.
- symbolic dynamics
- chaos; example of an itinerary of the forced pendulum.

Existence of Transversal Homoclinic Orbits

The Flow Mappings in the Interior and Exterior Regions of the Energy Surface.

- Recall some things about the Hill's regions. We consider the equations for the PCR3BP on the energy surface given by setting the energy equal to a constant.
- Let $\mathcal{M}$ be that energy surface, i.e.,

$$\mathcal{M}(\mu, C) = \{(x, y, \dot{x}, \dot{y}) \mid C(x, y, \dot{x}, \dot{y}) = \text{constant}\}$$

- The projection of this surface onto position space is a ***Hill's region***

$$M(\mu, C) = \{(x, y) \mid \Omega(x, y) \geq C/2\}.$$

In other terms, this reads

$$M(\mu, E) = \{(x, y) \mid U^{\text{eff}}(x, y) \leq E\}.$$

- The boundary of $M(\mu, C)$ is the ***zero velocity curve***. The comet can move only within this region in the (x, y)-plane. For a given μ recall (Lecture 2A) that there are five basic configurations for the Hill's region, the first four of which are shown in Figure 1.

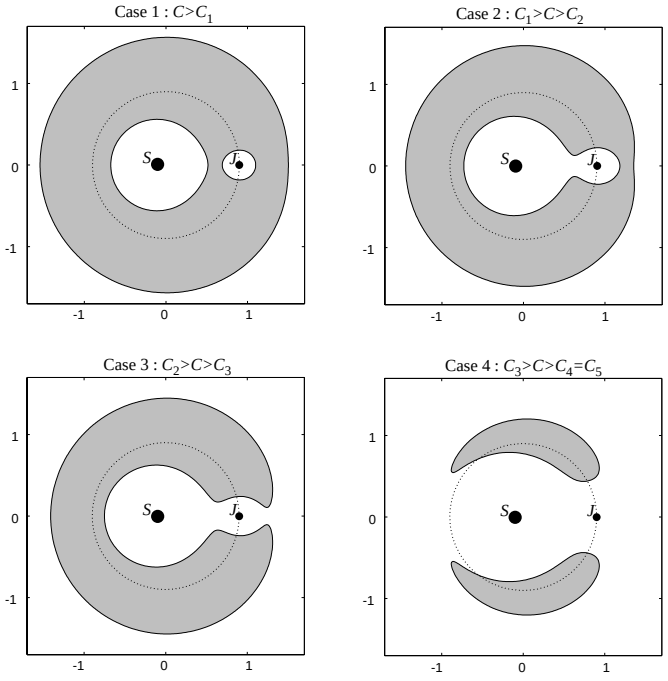

FIGURE 1: Four basic configurations of the Hill's region.

- Case 5 is where the comet is free to move in the entire plane.
- The shaded region is where the motion is ***forbidden***.
- The small oval region on the right is the ***Jupiter region***.
- The large near circular region on the left is the ***interior region*** surrounding the Sun.
- The region which lies outside the shaded forbidden region is the ***exterior region*** surrounding the Sun (and Jupiter).
- The values of C which separate these five cases will be denoted $C_i, i = 1, 2, 3, 4$ which are the values corresponding to the equilibrium points. These values can be easily calculated for small μ and their graphs are shown in Figure 2.
- For case 3, the Jacobi constant lies between C_2 and C_3 which are the Jacobi constants of the libration points L_2 and L_3 respectively.

In this case, the Hill's region contains a neck around both L_1 and L_2 and the comet can transit from the interior region to the exterior region and vice versa.

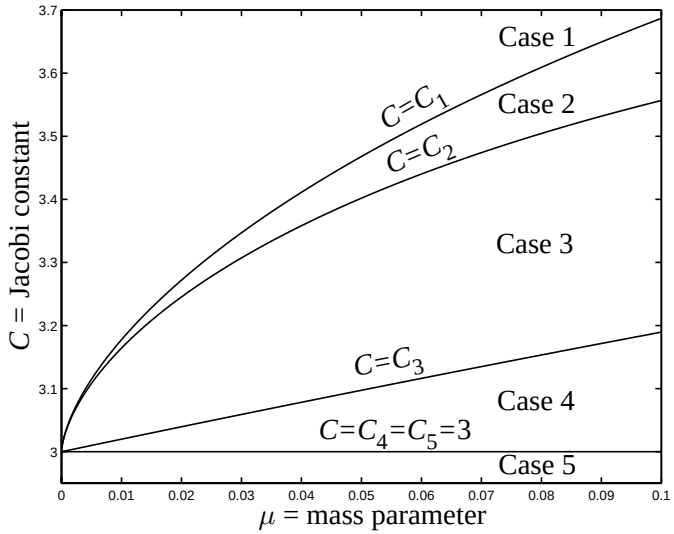

FIGURE 2: The partition of the (μ, C)-plane into five types of Hill's regions.

References

We are now going to study some work of Conley, McGehee and the Barcelona group. The references are:

- Conley, C. [1963] On some new long periodic solutions of the plane restricted three body problem. *Comm. Pure Appl. Math.* **16**, 449–467.
- Conley, C. [1968] Low energy transit orbits in the restricted three-body problem. *SIAM J. Appl. Math.* **16**, 732–746.
- McGehee, R. P. [1969] Some homoclinic orbits for the restricted three-body problem, Ph.D. thesis, University of Wisconsin.
- Libre, J., R. Martinez and C. Simó [1985] Transversality of the invariant manifolds associated to the Lyapunov family of perodic orbits near L2 in the restricted three-body problem, *Journal of Differential Equations* **58**, 104-156.

Code name: LMS [1985].

Orbit Segments Winding around a Solid Torus.

- In McGehee [1969], the energy surface is broken up further into regions bounded by invariant tori.
- These invariant tori project onto the darkly shaded annuli shown for case 3 in Figure 3.

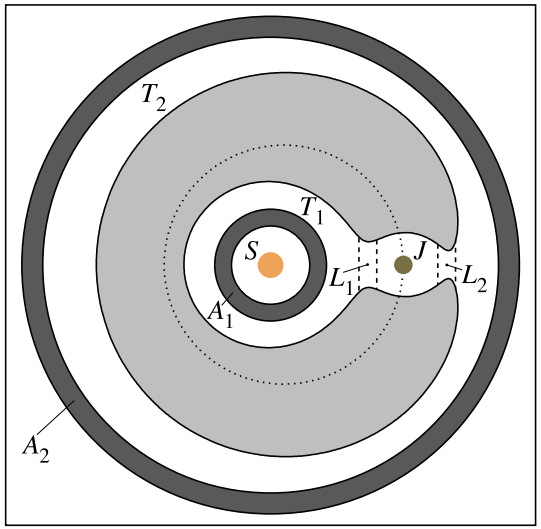

FIGURE 3: The projection of invariant tori (darkly shaded) on position space for case 3.

- These annuli separate the Hill's region into sections corresponding to invariant regions in the energy surface.
- For all of these cases the Sun and Jupiter are separated from each other by an invariant torus (although we show only case 3), thus making it impossible for the comet to pass from the Sun to Jupiter.
- Similarly, the two masses are separated from infinity by an invariant torus.
- We consider the regions of the energy surface projecting to the area between the two darkly shaded annuli, A_1 and A_2, i.e., the region containing Jupiter.
- The theorems of McGehee below show that all orbits leaving the vicinity of one of the unstable periodic orbits proceed around the annulus T_1 or T_2 before returning to that vicinity.
- The direction of procession is the same for all orbits, counterclock-

wise in the interior region and clockwise in the exterior region.

- In Lecture 2B we studied the regions near the unstable periodic orbits to obtain a qualitative picture of the orbits. We shall combine this picture of asymptotic orbits with the fact that orbits in the tori wind around in one direction *to construct homoclinic orbits* in both the interior and exterior regions. See Figure 4.

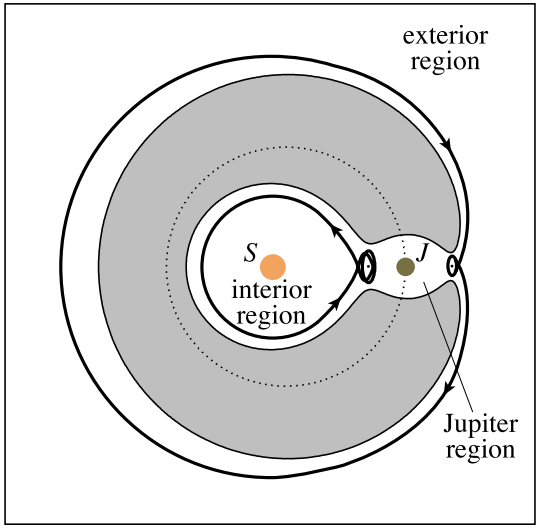

FIGURE 4: Homoclinic orbits in the interior and exterior regions.

Theorems of McGehee.

- To state the theorems, we first divide up the Hill's region and the energy surface.
- For small μ the two equilibrium points occur at a distance $\tilde{\mu}$ on either side of Jupiter with

$$\tilde{\mu} = \frac{2\mu^{1/3}}{3}.$$

- We isolate these points by drawing vertical lines on each side of them, i.e., lines at $(1 - \mu \pm c_1\tilde{\mu}, 0)$ and $(1 - \mu \pm b_1\tilde{\mu}, 0)$, where $b_1 < 1 < c_1$. This divides the Hill's region into five sets as shown in Figure 5.

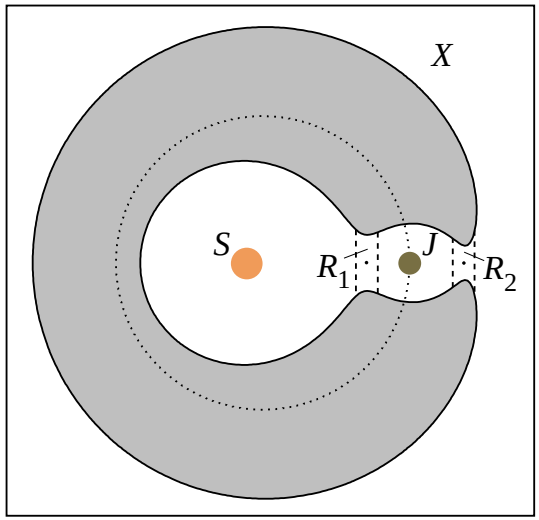

FIGURE 5: Division of Hill's region into five sets.

- Let S and J be the regions that contain the Sun and Jupiter; let region R_1 and region R_2 be those parts that contain the two equilibrium points L_1 and L_2, respectively; and let X be the region that lies exterior to the orbit of Jupiter.
- We also divide the energy surface $\mathcal{M}$ into sets projecting onto the regions shown in Figure 5. We keep the same name: e.g., region

$\mathcal{R}_1$ for the set in the energy surface whose projection is the region R_1 in the position space. The theorem below asserts that *one can choose the division described above so that we simultaneously have sufficient control of the flow in both regions* $\mathcal{S}$ *and* $\mathcal{R}_1$ *to construct a homoclinic orbit. The following theorem makes the same assertion for regions* $\mathcal{X}$ *and* $\mathcal{R}_2$.

- The analysis of regions $\mathcal{R}_1$ and $\mathcal{R}_2$ is of a local nature. In fact, we limit ourselves to those values of the Jacobi constant for which the linearized equations about the equilibrium point give us the qualitative picture of the flow.
- For b_1 and c_1 close to 1, i.e., for the region $\mathcal{R}$ close to the periodic orbit, the flow in $\mathcal{R}$ (which stands for both $\mathcal{R}_1$ and $\mathcal{R}_2$) can be described precisely (Lecture 2B). But we also know that we cannot make c_1 arbitrarily large without disturbing this qualitative picture for $\mathcal{R}$. On the other hand, we would like to make c_1 large enough

to obtain accurate estimates on the behavior of the flow in $\mathcal{S}$ and $\mathcal{X}$.

- The following theorems show that there exists a c_1 which allows us to balance these two factors.

Refer to Figure 6 while reading this theorem.

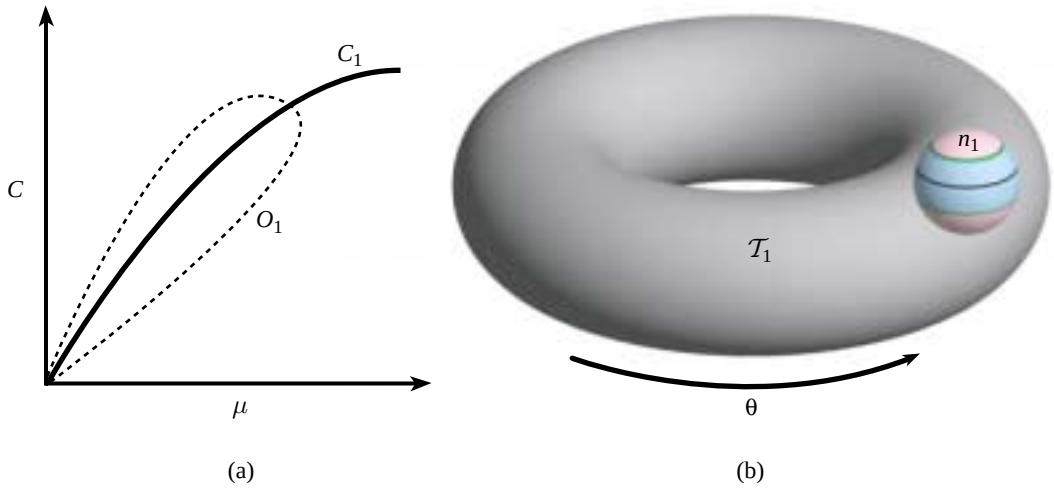

FIGURE 6: (a) Open set O_1 in (μ, C)-plane. (b) The invariant torus.

Theorem 1 (McGehee Interior Theorem) *There exist constants b_1 and c_1 and an open set O_1 in the (μ, C)-plane containing the graph of $C = C_1(\mu)$ for small $\mu > 0$ such that, for $(\mu, C) \in O_1$:*

1. *The energy surface $\mathcal{M}(\mu, C)$ contains an invariant torus separating the Sun from Jupiter.*
2. *For $C < C_1(\mu)$, the flow in $\mathcal{R}_1(\mu, C)$ is qualitatively the same as the flow for the linearized equations.*
3. *If we let $\mathcal{T}_1$ be that submanifold of $\mathcal{M}$ co-bounded by the invariant torus and n_1, then there is a function*

$$\theta : \mathcal{T}_1 \to \mathbb{R}$$

such that :

(a) *θ is a meridional angular coordinate for $\mathcal{T}_1$;*

(b) *θ is strictly increasing along orbits.*

Theorem 2 (McGehee Exterior Theorem) *There exist constants b_1 and c_1 and an open set O_2 in the (μ, C)-plane containing the graph of $C = C_2(\mu)$ for small $\mu > 0$ such that, for $(\mu, C) \in O_2$:*

1. *The energy surface $\mathcal{M}(\mu, C)$ contains an invariant torus separating the Sun and Jupiter from infinity.*
2. *For $C < C_2(\mu)$, the flow in $\mathcal{R}_2(\mu, C)$ is qualitatively the same as the flow for the linearized equations.*
3. *If we let $\mathcal{T}_2$ be that submanifold of $\mathcal{M}$ co-bounded by the invariant torus and n_2, then there exists a function*

$$\theta : \mathcal{T}_2 \to \mathbb{R}$$

such that :

(a) *θ is a meridional angular coordinate for $\mathcal{T}_2$;*

(b) *θ is strictly increasing along orbits.*

Existence of Orbits Homoclinic to the Lyapunov Orbit

- Part 3 of the above theorems gives us the following properties for the flow in $\mathcal{T}$ where $\mathcal{T}$ stands for either $\mathcal{T}_1$ or $\mathcal{T}_2$.
  - The increase in θ along an orbit segment in $\mathcal{T}$ with endpoints in the bounding sphere n is close to a non-zero integer multiple of 2π.
  - The increase in θ along any other orbit segment which can be deformed to the first, keeping both endpoints in the bounding sphere n, is close to the same integer multiple of 2π.
  - Furthermore, the increase of θ along any orbit segment remaining for an arbitrarily long time in $\mathcal{T}$ is arbitrary large.
- These are precisely the properties one needs to carry out the proof of the existence of a homoclinic orbit.

■ **A Dichotomy.** We assert that *either a transverse homoclinic orbit exists, or "total degeneracy" occurs.* Total degeneracy is the case when every orbit asymptotic to the unstable periodic orbit at one end is also asymptotic at the other end and hence is a homoclinic orbit. In other words, the total degeneracy situation occurs when the stable and unstable manifolds of the Lyapunov orbit coincide with each other. In either event we conclude the existence of a homoclinic orbit.

Sketch the proof. For more details, see Conley [1968] and McGehee [1969].

Assume that total degeneracy does not occur. The first step of the proof is to find an orbit segment in $\mathcal{T}_1$ connecting either d_1^- to a_1^+ or a_1^- to d_1^+ as follows. See Figure 7. Since $\mathcal{T}_1$ is compact and our flow, which is Hamiltonian, preserves a nondegenerate area element, we can conclude that some orbit which crosses $\mathcal{R}_1$ (and the bounding sphere n_1) and so enters $\mathcal{T}_1$ must also leave $\mathcal{T}_1$ and recross $\mathcal{R}_1$ (and n_1) the other way. See Figure 7. Therefore, for some point $p \in d_1^-$ of n_1, there is an orbit segment connecting p to a point $q \in d_1^+$ of n_1. Recall that in $\mathcal{R}_1$, the spherical caps d_1^- and d_1^+ are where the flow crosses n_1.

Starting with this orbit segment connecting p to q, we can find an orbit segment connecting either d_1^- to a_1^+ or a_1^- to d_1^+ as follows. Let γ be an arc in d_1^- linking p to a_1^- (where $\gamma \cap a_1^-$ is not on a

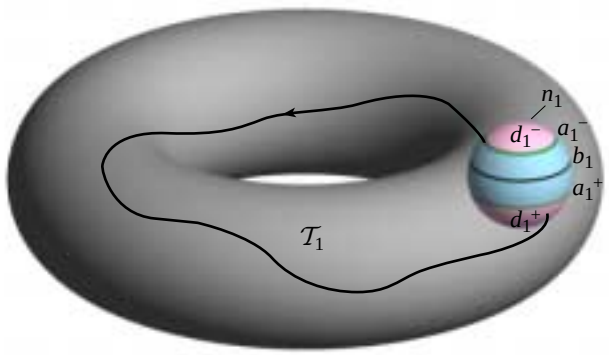

FIGURE 7: The existence of orbits homoclinic to the Liapunov orbit.

homoclinic orbit). If all of γ is carried by the flow to the spherical cap d_1^+, then we shall have an orbit segment with one endpoint in a_1^- and the other in d_1^+. Otherwise, starting from p, there is some maximal initial half-open subarc γ' of γ which is carried by the flow to d_1^+. Let r be the first point of γ not in γ', then the orbit segment with one endpoint at r must become arbitrarily long. But the only way this orbit segment can become arbitrarily long is to approach the asymptotic set, since the number of times it can wind around $\mathcal{T}_1$ is finite and therefore must contain an arbitrarily long subsegment in $\mathcal{R}_1$. Because of our knowledge of the flow in $\mathcal{R}_1$, we know that long orbit segments in $\mathcal{R}_1$ must lie close to the cylinders of asymptotic orbits and therefore r must be carried to a_1^+. Hence, in either case we conclude that there is an orbit segment connecting the set $d_1^\pm$ in one hemisphere

to the set of asymptotic orbits in the other.

Now, without loss of generality, we can suppose that we have found an orbit segment with one endpoint, called α, in a_1^- and the other in d^+. We now choose for γ the whole set a_1^-. Using arguments similar to the above, we can conclude that either all of a_1^- is carried by the flow inside d_1^+, or there exists a point $\beta \in a_1^-$ such that the orbit segment with β as an endpoint becomes asymptotic at the other end. If the first possibility holds, we would have a map of d^- to the interior of d^+, contradicting area preservation of Hamiltonian flow. Thus we have proven that either transversal homoclinic orbits exist or total degeneracy occurs for the interior region. The same proof also works for the exterior region.

Transversal Homoclinic Orbits in the Interior Region.

Conley [1968] and McGehee [1969] did not settle the issue of when one has transversality of the homoclinic orbit families for the PCR3BP. Subsequently, the Barcelona group (LMS [1985]) devoted their major effort to show that under appropriate conditions, the invariant manifolds of the L_1 Lyapunov orbits do meet transversally. We first establish some notation.

- Recall that near L_1 and for values of $C_1 > C > C_2$ (case 2), there is a family of unstable Lyapunov orbits.
- When C approaches C_1 from below, the periodic orbit tends to L_1.
- There are one-dimensional invariant stable, $W^s_{L_1}$, and unstable, $W^u_{L_1}$, manifolds associated to L_1.
- In a similar way, the L_1 Liapunov orbit has two-dimensional invariant manifolds $W^s_{L_1,\text{p.o.}}, W^u_{L_1,\text{p.o.}}$, locally diffeomorphic to cylinders.

- We recall that a homoclinic orbit related to an equilibrium point L or to a periodic orbit $\bar{L}$ is an orbit which tends to L (or $\bar{L}$) as $t \to \pm\infty$. Therefore, it is on the stable and unstable invariant manifolds of the related object (L or $\bar{L}$).
- A homoclinic orbit is called ***transversal*** if at some point of the orbit the tangent spaces to the stable and unstable manifolds at that point span the full tangent space to $\mathcal{M}(\mu, C)$ at the same point.
- The PCR3BP equations have the following symmetry

$$s : (x, y, \dot{x}, \dot{y}, t) \to (x, -y, -\dot{x}, \dot{y}, -t). \tag{1}$$

Therefore, if we know the unstable manifold of L_1 or of the Lyapunov orbit (which is a symmetrical periodic orbit) the corresponding stable manifold is obtained through the use of the stated symmetry. This observation will be used to find the transversal

homoclinic orbits.

The results below imply that for sufficiently small μ and for an appropriate range of $\Delta C = C_1 - C$, the invariant manifolds $W^{s,\mathcal{S}}_{L_1,\text{p.o.}}$ and $W^{u,\mathcal{S}}_{L_1,\text{p.o.}}$ in the interior region $\mathcal{S}$ intersect transversally.

Theorem 3 (First LMS Theorem) *For μ sufficiently small, the branch $W^{u,\mathcal{S}}_{L_1}$ of $W^{u}_{L_1}$ in the interior region $\mathcal{S}$ has a projection on position space (see Figure 8(a)) given by*

$$d = \mu^{1/3}\left(\frac{2}{3}N - 3^{1/6} + M\cos t + o(1)\right),$$
$$\alpha = -\pi + \mu^{1/3}(Nt + 2M\sin t + o(1)),$$

where d is the distance to the zero velocity curve, α is the angular coordinate and N and M are constants.

In particular, for a sequence of values of μ which have the following asymptotic expression:

$$\mu_k = \frac{1}{N^3 k^3}(1 + o(1)), \tag{2}$$

the first intersection of this projection with the x-axis is orthogonal to that axis, giving a symmetric (1,1)-homoclinic orbit for L_1. The prefix (1,1) refers to the first intersection (with the Poincaré section defined by the plane $y = 0, x < 0$) of both the stable and unstable manifolds of L_1.

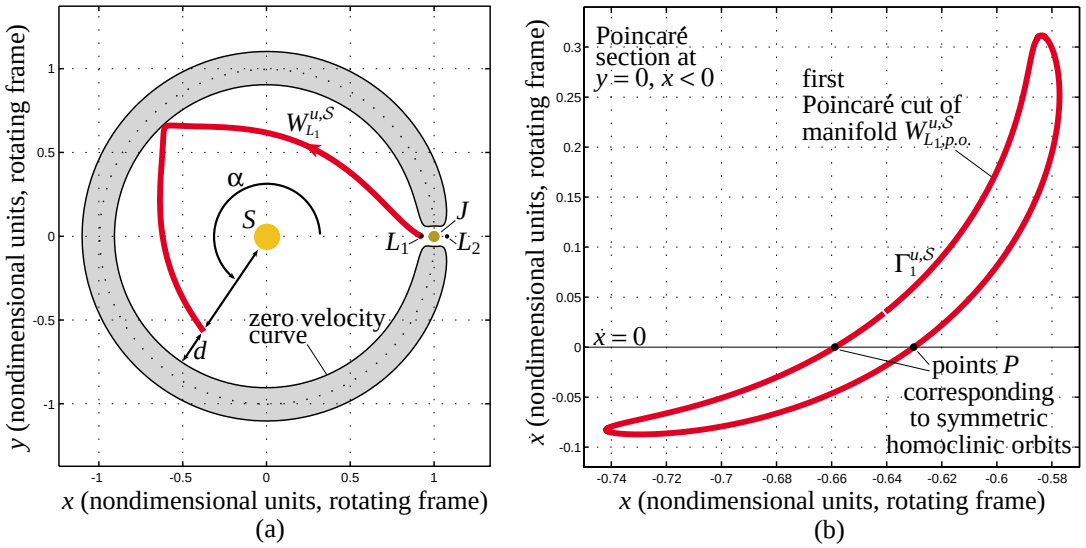

FIGURE 8: (a) Projection of the interior branch of the manifold $W^u_{L_1}$ on the position space. (b) First intersection (Poincaré "cut") $\Gamma_1^{u,\mathcal{S}}$ of the interior branch of $W^u_{L_1,\text{p.o.}}$ with the plane $y = 0$ in the region $x < 0$.

Theorem 4 (Second LMS Theorem) *For μ and $\Delta C = C_1 - C$ sufficiently small, the branch $W^{u,\mathcal{S}}_{L_1,\text{p.o.}}$ of $W^u_{L_1,\text{p.o.}}$ contained initially in the interior region $\mathcal{S}$ of the energy surface intersects the plane $y = 0$ for $x < 0$ in a curve diffeomorphic to a circle (see*

Figure 8(b)).

In particular, for points in the (μ, C) *plane such that there is a* μ_k *of the preceding Theorem for which*

$$\Delta C > L\mu_k^{4/3}(\mu - \mu_k)^2 \tag{3}$$

holds (where L *is a constant), there exist symmetric transversal (1,1)-homoclinic orbits.*

For details of the proofs, see LMS [1985], but we need to make a few relevant comments.

- The main objective of both theorems is to study the transversality of the invariant manifolds for the L_1 Lyapunov orbit on the energy surface whose Jacobi constant C is slightly less than $C_1(\mu)$ as one varies μ and C. The main step is to obtain an expression for the first intersection $\Gamma_1^{u,\mathcal{S}}$ of the unstable manifold $W_{L_1,\text{p.o.}}^{u,\mathcal{S}}$ with the

plane $y = 0$ in the region $x < 0$. While formulas were provided in LMS [1985] for this closed curve as a function of μ and ΔC in the variables $x, \dot{x}$, they are quite complicated and difficult to interpret and hence are not included here. But the key point is the following. According to the first LMS Theorem, the set of values of μ for which we have a symmetric (1,1)-homoclinic orbit associated to L_1 is discrete and is given by equation (2). Then for any other value of μ the unstable manifold $W^{u,\mathcal{S}}_{L_1}$ of L_1 reaches the $(x, \dot{x})$-plane in a point $(x_1, \dot{x}_1)$ outside $\dot{x} = 0$. Therefore, if ΔC is too small, $\Gamma^{u,\mathcal{S}}_1$ does not cut the x-axis and hence (by symmetry) $\Gamma^{s,\mathcal{S}}_1$ of the stable manifold $W^{s,\mathcal{S}}_{L_1,\text{p.o.}}$ does not cut the x-axis either. Therefore the first intersections of the invariant manifolds do not meet and there is no symmetric (1,1)-homoclinic orbit.

However, for a fixed value of μ, if we increase ΔC, we hope that

$\Gamma_1^{u,\mathcal{S}}$ of the unstable manifold will become large. Therefore we can look for some value of ΔC such that $\Gamma_1^{u,\mathcal{S}}$ becomes tangent to the x-axis or even intersects it at more than one point. Then, due to the reversibility of the PCR3BP, $\Gamma_1^{s,\mathcal{S}}$ of the stable manifold also intersects the x-axis at the same points. Points P on the x-axis where $\Gamma_1^{u,\mathcal{S}}$ and $\Gamma_1^{s,\mathcal{S}}$ intersect correspond to (symmetric) orbits homoclinic to the Lyapunov orbit (see Figure 8(b)). If $\Gamma_1^{u,\mathcal{S}}$ is transversal to $\Gamma_1^{s,\mathcal{S}}$ at P then the homoclinic orbit is transversal. The results of the second LMS Theorem say that the above phenomenon occurs if $\Delta C > L\mu_k^{4/3}(\mu - \mu_k)^2$ holds.

- Using the results of the second LMS Theorem one can draw a mesh of homoclinic tangencies for the $(\mu, \Delta C)$-plane. The numbers in Figure 9 show the number of symmetric (1,1)-homoclinic points

found in the first intersection of $W^{u,\mathcal{S}}_{L_1,\text{p.o.}}$ with the plane $y = 0, x < 0$ when one varies μ and ΔC. For us, the key point of the theorems is that for the wide range of μ which exist in the solar system, the invariant manifolds of the L_1 Lyapunov orbit intersect transversally for sufficiently large ΔC.

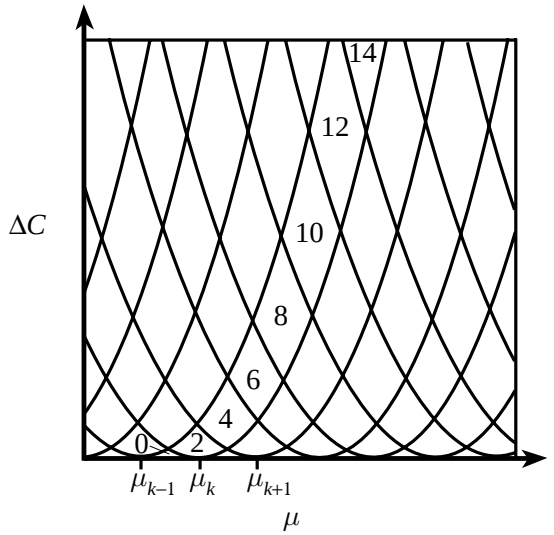

FIGURE 9: Partition of the $(\mu, \Delta C)$-plane according to the number of symmetric (1,1)-homoclinic points found in the first intersection of $W^{u,\mathcal{S}}_{L_1,\text{p.o.}}$ with the plane $y = 0, x < 0$.

- The heart of the proofs of these two theorems is to obtain expressions for $W_{L_1}^{u,\mathcal{S}}$ as a function of μ and for $W_{L_1,\text{p.o.}}^{u,\mathcal{S}}$ as a function of μ and ΔC. By using the basic framework of McGehee [1969], LMS [1985] divided the annulus T_1 in the interior region S into two parts: a small neighborhood H near R_1 and the rest of the region outside this small neighborhood. In the neighborhood H, the PCR3BP can be considered as a perturbation of the Hill's problem. In celestial mechanics, it is well known that Hill's problem studies the behavior near the small mass of PCR3BP in the limit when μ approaches zero. In the rest of the region away from the small mass, the PCR3BP can be approximated by the two-body problem in a rotating frame. Through a number of careful estimations, LMS [1985] were able to obtain these analytical results.

Summary.

- Conley [1968] and McGehee [1969] proved the existence of homoclinic orbits for both the interior and exterior region.
- LMS [1985] have shown analytically the existence of transversal symmetric (1,1)-homoclinic orbits in the interior region under appropriate conditions. But this is for ***Case 2***!
- For our problem, we need to find transversal homoclinic orbits in both interior and exterior regions and transversal heteroclinic cycles for the L_1 and L_2 Lyapunov orbits. To do this, we perform some numerical explorations using the tools developed by the Barcelona group. Reference:

- Gómez, G., A. Jorba, J. Masdemont, and C. Simó [1991] Study Refinement of Semi-Analytical Halo Orbit Theory, Final Report, *ESOC Contract No.: 8625/89/D/MD(SC)*, Barcelona, April, 1991.

Existence of the Chain

- Where are we?
- To proceed with the problem of interest to us (Case 3), we need to get transverse homoclinic orbits in the interior, exterior and the Jupiter region.
- These results are, unfortunately, ***not available analytically***, so we are going to proceed numerically.

Transversal Homoclinic Orbits in the Exterior Region.

- We turn our attention now to numerical explorations of the problem, and in particular, to the existence of transversal homoclinic orbits for the L_2 Lyapunov orbit in the exterior region.
- Though there are no analytical results proving the existence of transversal homoclinic orbits in the $\mathcal{X}$ region, we can construct them numerically by finding an intersection of the manifolds $W^s_{L_2,\text{p.o.}}$ and $W^u_{L_2,\text{p.o.}}$ on an appropriately chosen Poincaré section.
- Numerical experiments guided by geometrical insight suggest that we cut the flow by the plane $y = 0$, the line passing through the two masses in the rotating frame. The branch of the manifold $W^u_{L_2,\text{p.o.}}$ which enters the $\mathcal{X}$ region flows clockwise in the position space. We refer to this exterior branch of the manifold as $W^{u,\mathcal{X}}_{L_2,\text{p.o.}}$. See Figure 10(a).

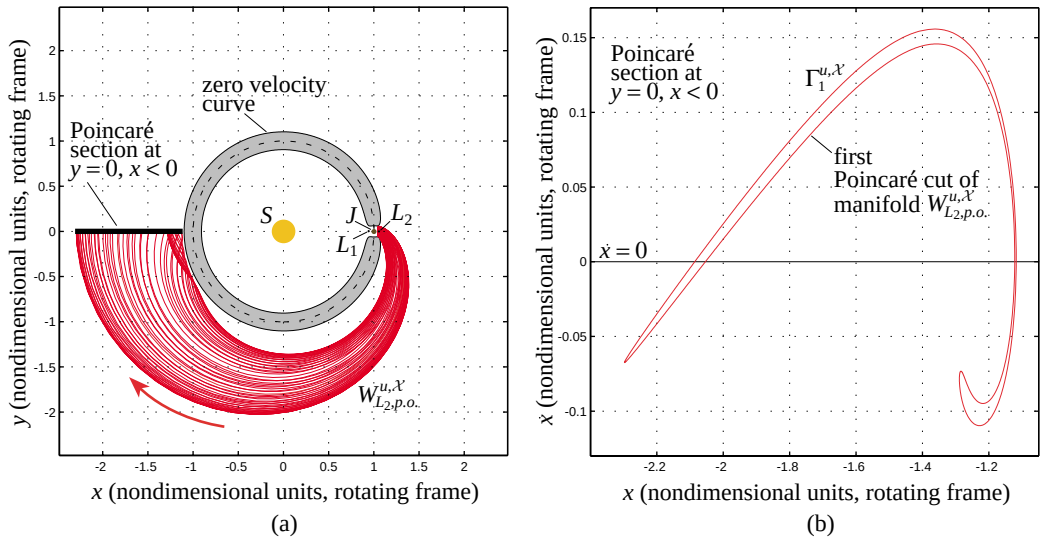

FIGURE 10: (a) The position space projection of the unstable manifold "tube" $W^{u,\mathcal{X}}_{L_2,\text{p.o.}}$ until the first intersection with the Poincaré section at $y = 0, x < 0$. (b) The first Poincaré cut $\Gamma_1^{u,\mathcal{X}}$ of the manifold $W^{u,\mathcal{X}}_{L_2,\text{p.o.}}$ on the plane $y = 0, x < 0$.

- This two-dimensional manifold "tube" $W^{u,\mathcal{X}}_{L_2,\text{p.o.}}$ first intersects the plane $y = 0$ on the part of T_2 which is opposite to L_2 with respect to the Sun (i.e., $x < 0$).
- The intersection, as one would expect geometrically, is a curve

diffeomorphic to a circle. We call this intersection the first "cut" of $W^{u,\mathcal{X}}_{L_2,\text{p.o.}}$ with $y = 0$. See Figure 10(b).

- To define the first cut, we exclude a neighborhood of n_2 in the $\mathcal{X}$ region. Some arcs of this curve produce successive intersections without leaving the $\mathcal{X}$ region.
- The q-th of these intersections of $W^{u,\mathcal{X}}_{L_2,\text{p.o.}}$ with $y = 0$ will be referred to as $\Gamma^{u,\mathcal{X}}_q$. Similarly, we call $\Gamma^{s,\mathcal{X}}_p$ the corresponding p-th intersection with $y = 0$ of the exterior region branch of $W^s_{L_2,\text{p.o.}}$.
- A point in $y = 0$ belonging to $\Gamma^{u,\mathcal{X}}_q \cap \Gamma^{s,\mathcal{X}}_p$ (if not empty) will be called a (q,p)-***homoclinic point***. The existence of (q,p)-homoclinic points for certain q and p is shown in McGehee [1969].

- ***Next goal:*** obtain the first such transversal intersection of $\Gamma_q^{u,\mathcal{X}}$ with $\Gamma_p^{s,\mathcal{X}}$ and so obtain a transversal (q,p)-homoclinic point. Other intersections (for larger q and p) may exist, but we will restrict ourselves for now to the first.
- Suppose that the unstable manifold intersection $\Gamma_q^{u,\mathcal{X}}$ is a closed curve γ in the variables $x, \dot{x}$. Let s_x be the symmetry with respect to the x-axis on this plane. Then due to the reversibility of the PCR3BP, the q-th intersection $\Gamma_q^{s,\mathcal{X}}$ of the stable manifold $W_{L_2,\text{p.o.}}^{s,\mathcal{X}}$ with $y = 0$ is $s_x\gamma$. For some minimum q, the closed curve γ intersects the $\dot{x} = 0$ line of the $(x, \dot{x})$-plane.
- Points P along the curve γ which intersect the $\dot{x} = 0$ line are (q,q)-homoclinic points, corresponding to (symmetric) orbits homoclinic to the Lyapunov orbit. If the curve γ is transversal to the curve $s_x\gamma$ at the point P then the homoclinic orbit corresponding to P

is transversal. If intersections between the curves γ and $s_x\gamma$ exist off the line $\dot{x} = 0$ (i.e., if the set $(\gamma \cap s_x\gamma)\backslash\{\dot{x} = 0\}$ is nonempty), then nonsymmetric homoclinic orbits appear.

- Consider Figure 10(b), where we used the values $\mu = .0009537$ and $\Delta C = C_2 - C = .01$ to compute the unstable Poincaré cut. If we also plotted the stable cut $\Gamma_1^{s,\mathcal{X}}$, which is the mirror image of unstable cut $\Gamma_1^{u,\mathcal{X}}$, we would find several points of intersection.
- In Figure 11(a), we focus on the left-most group of points, centered at about $x = -2.07$. We find two $\dot{x} = 0$ intersections which are transversal homoclinic points in the $\mathcal{X}$ region. The transversal symmetric $(1,1)$-homoclinic orbit corresponding to the left $\dot{x} = 0$ intersection is shown in Figure 11(b).

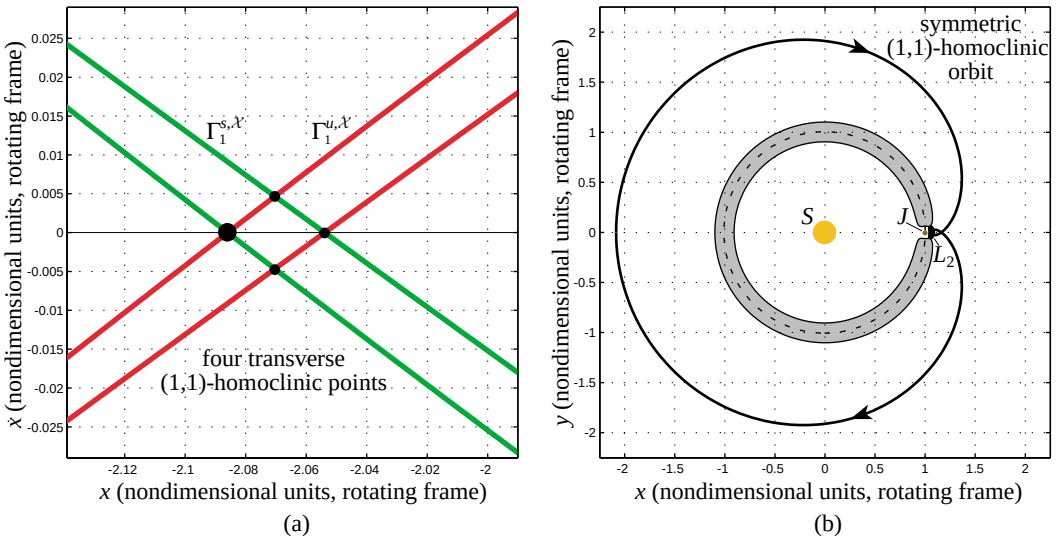

FIGURE 11: (a) A group of four transverse $(1,1)$-homoclinic points. (b) The symmetric $(1,1)$-homoclinic orbit corresponding to the left $\dot{x} = 0$ $(1,1)$-homoclinic point (the large black dot in (a)).

- Notice two off-axis intersections in Figure 11(a), completing the local transversal intersection of two closed loops in the $(x, \dot{x})$-plane.
- As these two intersections occur near the line $\dot{x} = 0$, they will be nearly symmetric. A more pronounced case of nonsymmetry occurs

for the other group of intersection points centered near $x = -1.15$, for which we have the nonsymmetric $(1, 1)$-homoclinic orbit given in Figure 12.

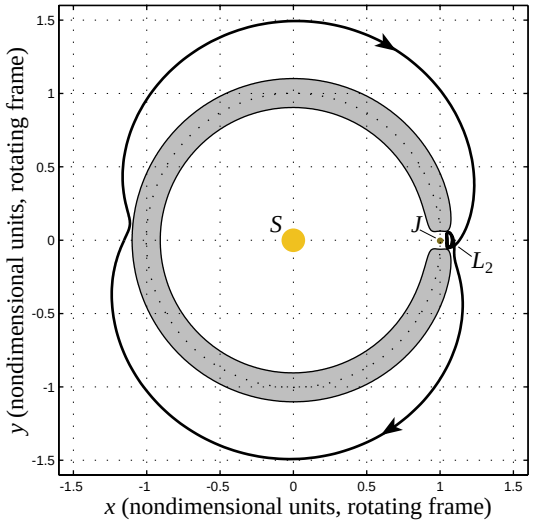

FIGURE 12: A nonsymmetric $(1, 1)$-homoclinic point.

- A similar procedure can numerically produce homoclinic orbits in the interior region as well as in the Jupiter region. We can even look at cuts beyond the first. See Figure 13(a).

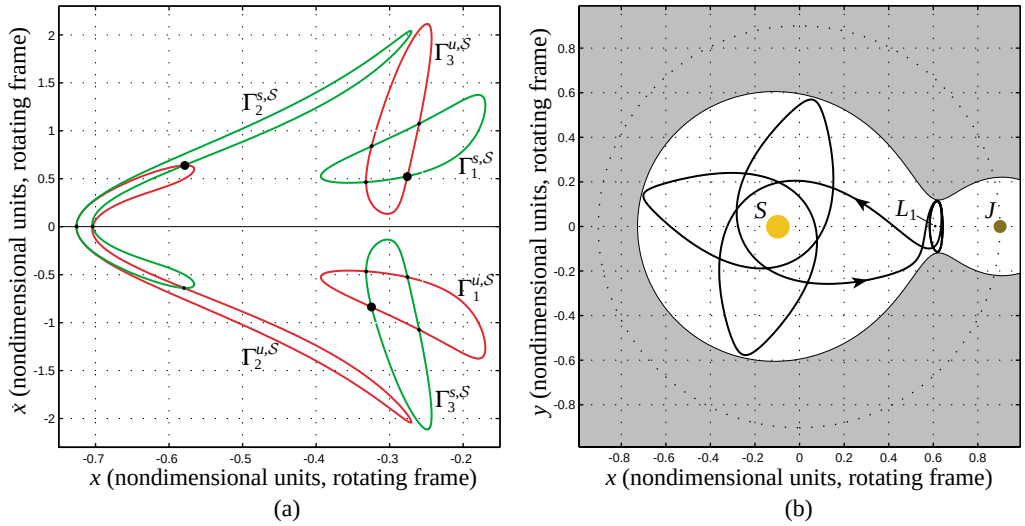

FIGURE 13: (a) The first three Poincaré cuts of the unstable ($W^{u,\mathcal{S}}_{L_1,\text{p.o.}}$) and stable ($W^{s,\mathcal{S}}_{L_1,\text{p.o.}}$) manifolds with the plane $y = 0$. (b) A nonsymmetric $(1,3)$-homoclinic orbit in the interior region (corresponding to the large dot in (a)).

- In Figure 13(b) we show an interior region $(1,3)$-homoclinic orbit

(note, also $(2,2)$ and $(3,1)$, using $\bar{q}+\bar{p}=q+p$) associated to an L_1 Lyapunov orbit for $\mu=.1, \Delta C = C_1 - C = .0743$.

Heteroclinic Connections between Lyapunov Orbits.

- We construct a heteroclinic connection between Lyapunov orbits of L_1 and L_2 by finding an intersection of their respective invariant manifolds in the $\mathcal{J}$ region.
- To do so, we seek points of intersection on a suitably chosen Poincaré section. For instance, to generate a heteroclinic orbit which goes from an L_1 Lyapunov orbit (as $t \to -\infty$) to an L_2 Lyapunov orbit (as $t \to +\infty$), we proceed as follows.
- We restrict ourselves for now to case 3 ($C_2 > C > C_3$, see Figure 1), for which the Hill's region opens enough to permit Lyapunov orbits about both L_1 and L_2 to exist.

- Let the branch of the unstable manifold of the L_1 Lyapunov orbit which enters the $\mathcal{J}$ region be denoted $W^{u,\mathcal{J}}_{L_1,\text{p.o.}}$.
- On the same energy surface (same C value) there is an L_2 Lyapunov orbit, whose stable manifold in the $\mathcal{J}$ region we shall similarly denote $W^{s,\mathcal{J}}_{L_2,\text{p.o.}}$.
- The projection of the two-dimensional manifold tubes onto the position space is shown in Figure 14(a).

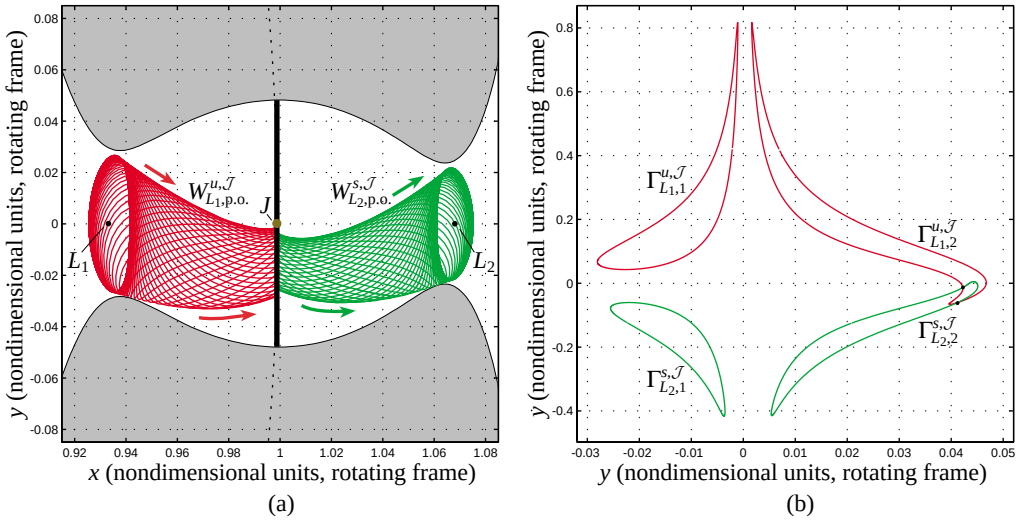

FIGURE 14: (a) The projection of invariant manifolds $W^{u,\mathcal{J}}_{L_1,\text{p.o.}}$ and $W^{s,\mathcal{J}}_{L_2,\text{p.o.}}$ in the region J of the position space. (b) The first two Poincaré cuts of the invariant manifolds with the plane $x = 1 - \mu$.

- To find intersections between these two tubes, we cut the flow by the plane $x = 1 - \mu$. See Figure 14(b).
- This convenient plane maximizes the number of intersections for values of μ, C which produce manifolds making a limited number of revolutions around Jupiter before escaping from the $\mathcal{J}$ region.

- The q-th intersection of $W^{u,\mathcal{J}}_{L_1,\text{p.o.}}$ with the plane $x = 1-\mu$ will be labeled $\Gamma^{u,\mathcal{J}}_{L_1,q}$. Similarly, we will call $\Gamma^{s,\mathcal{J}}_{L_2,p}$ the p-th intersection of $W^{s,\mathcal{J}}_{L_2,\text{p.o.}}$ with $x = 1-\mu$.
- Numerical experiments show that the L_1 Lyapunov orbit unstable manifold $W^{u,\mathcal{J}}_{L_1,\text{p.o.}}$ does not coincide with the L_2 Lyapunov orbit stable manifold $W^{s,\mathcal{J}}_{L_2,\text{p.o.}}$.
- For a wide range of μ and C values (where $(C_2 > C > C_3)$, numerical explorations show that ***they do intersect transversally***.
- While it is true that for certain values of μ and C, there are tangencies between the stable and unstable manifold, we will not deal with this interesting case in this study. Hence, from now on, we will concentrate our numerical explorations only on the cases where

the stable and unstable manifold intersect transversally.

- Now, suppose that $\Gamma^{u,\mathcal{J}}_{L_1,q}$ and $\Gamma^{s,\mathcal{J}}_{L_2,p}$ are each closed curves in the variables $y, \dot{y}$. A point in the plane $x = 1 - \mu$ belonging to the intersection of the two closed curves (i.e., $\Gamma^{u,\mathcal{J}}_{L_1,q} \cap \Gamma^{s,\mathcal{J}}_{L_2,p}$) will be called a (q,p)-***heteroclinic point*** because such a point corresponds to a heteroclinic orbit going from the L_1 Lyapunov orbit to the L_2 Lyapunov orbit.
- Our objective is to obtain the first intersection point (or group of points) of the curve $\Gamma^{u,\mathcal{J}}_{L_1,q}$ with the curve $\Gamma^{s,\mathcal{J}}_{L_2,p}$ and so obtain the minimum values of q and p such that we have a transversal (q,p)-heteroclinic point. Other intersections may exist, but we will restrict ourselves for now to the first.
- For some minimum q and p, we have an intersection of the curves, and some number of (q,p)-heteroclinic points, depending on the

geometry of the intersection. Note that the sum $q + p$ must be an even positive integer.

- As we are interested in heteroclinic points for the Sun-Jupiter system ($\mu = .0009537$), we took $C = 3.037$ and proceeded numerically to obtain the intersections of the invariant manifolds $W^{u,\mathcal{J}}_{L_1,\text{p.o.}}$ and $W^{s,\mathcal{J}}_{L_2,\text{p.o.}}$ with the plane $x = 1 - \mu$. In Figure 14(b) we show the curves $\Gamma^{u,\mathcal{J}}_{L_1,q}$ for $q = 1, 2$ and $\Gamma^{s,\mathcal{J}}_{L_2,p}$ for $p = 1, 2$. Notice that $\Gamma^{u,\mathcal{J}}_{L_1,2}$ and $\Gamma^{s,\mathcal{J}}_{L_2,2}$ intersect in two points (the black dots in Figure 14(b) near $y = .042$).
- Thus, the minimum q and p for a heteroclinic point to appear for this particular value of μ, C is $q = 2$ and $p = 2$. The $(2, 2)$-heteroclinic points can each be forward and backward integrated to produce heteroclinic trajectories going from the L_1 Lyapunov

orbit to the L_2 Lyapunov orbit. We show one of the heteroclinic orbits in Figure 15.

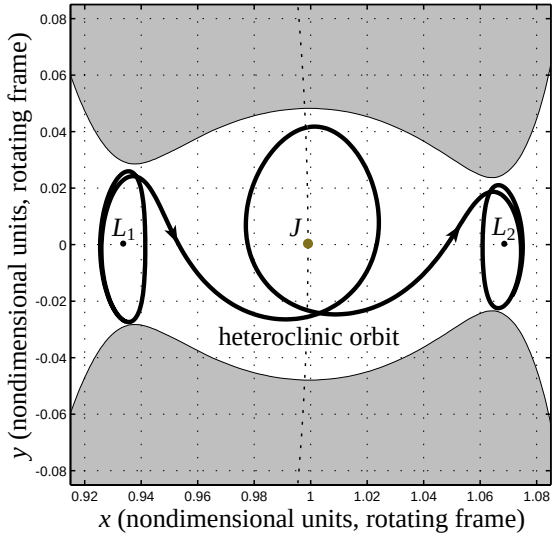

FIGURE 15: The existence of a transversal $(2, 2)$-heteroclinic orbit in the J region.

- The number of revolutions around Jupiter is given by $(q+p-1)/2$.
- The reverse trajectory, going from the L_2 Lyapunov orbit to the L_1 Lyapunov orbit, is easily given by the symmetry s (1).
- It would be the mirror image (about the x-axis) of the trajectory in Figure 15, with the direction arrows reversed. These two *heteroclinic connections* together form a symmetric ***heteroclinic cycle***.

Summary.

- We have used a combination of analytical and numerical techniques to show the existence of homoclinic and heteroclinic orbits associated to the L_1 and L_2 Lyapunov orbits for case 3.
- Combining homoclinic and heteroclinic orbits of the same Jacobi constant value, we generate a homoclinic/heteroclinic chain of orbits, which asymptotically connect the L_1 and L_2 Lyapunov orbits.
- These chains imply a complicated dynamics connecting the interior, exterior, and Jupiter regions.
- As an example, we again choose the Sun-Jupiter system ($\mu = .0009537$), but now a Jacobi constant value similar to that of comet *Oterma* during its Jupiter encounters ($C = 3.03$).
- We obtain an interior region orbit homoclinic to the L_1 Lyapunov orbit, an exterior region orbit homoclinic to the L_2 Lyapunov orbit,

and a heteroclinic orbit connecting the L_1 and L_2 Lyapunov orbits. The union of these orbits is a ***homoclinic-heteroclinic chain***. See Figure 16. This has important consequences, such as locating trajectories with given itineraries, explored in lecture 3B.

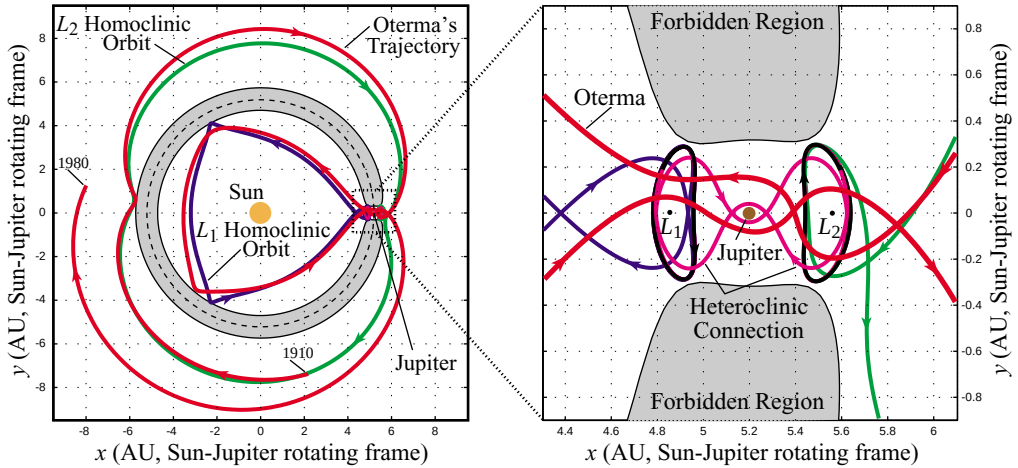

FIGURE 16: A dynamical channel (homoclinic-heteroclinic chain) corresponding to the Jupiter comet *Oterma*. The periodic orbits about L_1 and L_2 are black. Their homoclinic orbits are blue and green. The heteroclinic connection between them is magenta. The actual orbit of *Oterma* (AD 1910–1980) is shown in red overlaying the chain. Distances are in Astronomical Units (AU).